A Single-step Process of Generating Hollow and Porous TiO₂ Nanoparticles by Picosecond Laser Ablation in Deionised Water

Abubaker Hamad*, Lin Li*, Zhu Liu*,**, Xiang Li Zhong**

Laser Processing Research Centre, School of Mechanical, Aerospace and Civil Engineering, The University of Manchester, Manchester, M13 9PL, UK
Abubaker.hamad75@yahoo.co.uk
**School of Materials, The University of Manchester, Manchester M13 9PL, UK.*

Over the last two decades, hollow nanoparticles have received considerable attention from researchers due to their specific properties that do not appear in other forms of nanoparticles. It has been recognised that TiO₂ hollow nanoparticles have superior photocatalytic properties than solid TiO₂ nanoparticles. Previous methods of producing hollow TiO₂ nanoparticles typically involve multiple-steps. In this paper, we report the production of hollow and porous TiO₂ nanoparticles in a single step via high-repetition rate picosecond laser ablation in deionised water. The absorption spectra of the colloidal nanoparticles were obtained by UV-VIS spectroscopy. The size distribution and morphology were characterised by transmission electron microscopy (TEM). The morphology and chemical composition of the nanoparticles were characterised using a High-Angle Annular Dark-Field – Scanning Transmission Electron Microscope (HAADF-STEM) and Energy Dispersive X-ray Spectroscopy (EDS). In addition, the crystalline structures were investigated using X-ray diffraction (XRD). The results show that a higher ratio of crystalline hollow and porous TiO₂ nanoparticles (20 – 160 nm in size with majority of hollow nanoparticles at 20 nm and an average size of 37 nm) of mixed anatase, rutile and brookite phases, was produced at lower laser energy; the yield was increased from 8% to 25% by reducing the laser power from 9.12 W to 3.35 W respectively. High laser powers result in reduced energy gap in the nanoparticles produced. The work shows that laser power can be used to control the yield of hollow nanoparticles.

1. Introduction

Laser ablation in liquids has advantages including high material purity and being environmentally clean. In addition, using a suitable liquid (e.g. inorganic salts) or applying an electrical field, the size, shape and phase of the nanocrystals can be controlled [1]. Nanoparticles can be produced in an ambient condition without the need to provide high temperature (*T*) and pressures (*P*) [2].

Hollow nanoparticles have found a wide range of applications in the materials community and in cosmetics, coatings, composite materials, dyes, ink, artificial cells, microencapsulates for drug delivery [3], photodegradation of organic pollutants [4], cancer imaging and therapy [5]. Their popularity is due to their specific properties such as large specific areas [4], low density, good mechanical and thermal stabilities, and surface permeability [3].

Yang et al. [6] produced porous hollow TiO₂ nano-sphere particles using a facile hydrothermal method. It was concluded that the hollow nanoparticles show strong adsorption efficiency for organic dyestuff. Furthermore, they have optimal sensitivity to formaldehyde (HCHO) gas of the TiO₂ film sensor, enhanced at a comparatively low operating temperature (200 °C). Pang et al. [7] produced spherical sub-micrometer sized hollow TiO₂ particles by self-assembling directly from commercial TiO₂ nanoparticles. The hollow particles show "good visible light scattering match that significantly improve the photoconversion efficiency". Katagiri et al. [8] generated spherical hollow TiO₂ nanoparticles (with well-defined diameters) of the desired polymorphs via layer-by-layer formation of a water-soluble Ti complex on colloid complex and hydrothermal treatment. Tsai et al. [9]

produced spherical hollow TiO₂ particles via a self-sacrificing template method. They concluded that the small hollow sphere particles have higher absorption ability than larger hollow particles because the smaller particles have thinner shells. The small hollow TiO₂ particles exhibited enhanced photocatalytic activity against photodegradation of methylene blue (MB).

Hollow nanoparticles are of particular interest to materials science and catalytic applications. Chaudhuri and Paria, [4] prepared hollow TiO₂ nanoparticles during the production of sulphur-doped TiO₂ nanoparticles. It was shown that the hollow TiO₂ nanoparticles had greater photocatalytic activity under normal light against methylene blue in comparison with the standard Degussa P25 TiO₂ nanoparticle. This is because hollow TiO₂ nanoparticles have a lower energy band gap and a higher specific surface area, 2.5 eV and 318.11 m²g⁻¹ respectively, in comparison with solid TiO₂ nanoparticles (3.2 eV and 130.94 m²g⁻¹ respectively). Wang et al. [10] observed the production of hollow TiO₂ nanoparticles while generating polystyrene/titanium dioxide (PSt/TiO₂) core-shell composite nanoparticles in a mixed solution (ethanol and water) using the hydrolysis method. Hollow TiO₂ nanoparticles were produced after calcinations of the PSt/TiO₂ core-shell particles to remove or burn off the PSt core or using tetrahydrofuran (THF) to decay the core. The results show that the hollow TiO₂ nanoparticles produced after calcinations had the highest photocatalytic efficiency against degradation of Rhodamine B (RB).

In addition to hollow TiO₂ nanoparticles, some other types of hollow nanoparticles have also been produced for use in different fields; Smovzh, [11] produced hollow Al₂O₃ (γ-phase Al) nanoparticles via electric-arc sputtering of a

composite electrode in helium gas followed by annealing in oxygen or oxidation. The nanoparticles produced were 6-12 nm in size, with a thickness of approximately 2-3 nm. Khanal et al. [3] produced hollow silica nanoparticles via a template of triblock copolymer micelle with a core-shell-corona architecture. The method can produce tuneable thickness of nanoparticles by changing the concentration of the inorganic precursors. Ming et al. [12] produced dense hollow porous Co_3O_4, FeO_x, NiO and MnO_x metal oxide nanoparticles with a size of less than 100 nm by a hard-template method. These types of nanoparticles enhanced the active surface area; for example, Co_3O_4 nanoparticles are useful for promoting electrochemical reactions in lithium-ion batteries, leading to greater productivity. A high discharge voltage and low charge potential were also observed (about 2.74 V and 4.0 V respectively). In addition, a long cycle ability (more than 100 cycles) at a delivered capacity of 2000 mA h g^{-1} was also noted. Niu et al. [13] produced metal oxide and sulphide hollow nanoparticles by laser ablation in a liquid environment. The hollow nanoparticles were produced by the following two steps based on the Kirkendall effect and IR laser vaporisation; In the first step, the Kirkendall effect was used to produce hollow nanoparticles with fast metal diffusivity in the metal oxide shell such as oxide/sulphide shell. In the second step, an IR laser was used to vaporise the metal core with a slow metal diffusivity to the shell of the nanoparticles. ZnS hollow nanoparticles enhanced gas sensors. It was also reported that the nanostructures, including heterostructure, compound nanospheres and spherical core-shell form can be enhanced via suitable selection of liquid environment and target material. Lee et al. [14] prepared double-shell SiO_2/TiO_2 hollow nanoparticles by a chemical method. It was concluded that the double-shell hollow nanoparticles based on Electrorheological (ER) fluids showed promising enhanced ER qualities in comparison with the single-shell hollow nanoparticles based on ER fluids. ER performance is increased by decreasing the particle size due to increasing surface area.

Yang et al. [15] produced nano-crystalline diamond, having a hexagonal lattice or cubic lattice, by high-power pulsed laser ablation of a graphite target in water. It demonstrated that the compounds that would require extreme conditions general, can be generated at normal temperature and pressure by using the pulsed-laser-induced reactive quenching (PLIRQ) method. Yang and Wang [16] produced carbon nitride nanocrystals by pulsed laser induced liquid–solid interfacial reaction (PLIIR). They observed a cubic-C_3N_4 phase in carbon nitride nanocrystals.

From the above review, it is clear that the production of hollow and porous nanoparticles mainly involves multiple steps and the proportion of porous or hollow nanoparticles is not generally controllable. In this work, the authors demonstrate a controllable one-step synthesis of hollow TiO_2 nanoparticles via a picosecond laser ablation process in deionised water.
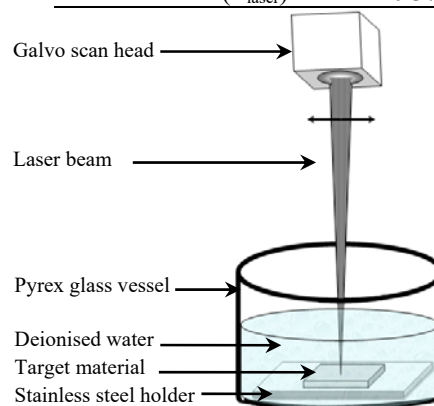
2. Experimental set-up

2.1 Nanoparticle production

A 99.99+% pure titanium (Ti) plate with dimensions of 25 mm × 25 mm × 1 mm was used to synthesise TiO_2 nanoparticles by a picosecond laser in deionised water. A Ti plate was placed at the bottom of a glass vessel on a stainless steel substrate (see Fig. 1). The water level above the target was approximately 2 mm. A 400 W Edgewave pulsed laser (picosecond laser: parameters are shown in Table 1) was used for the ablation process. The laser ablation process in deionised water was conducted continually for 10 minutes. Because water has a significant absorption at a wavelength of 1064 nm, the effects of the water level on the laser beam energy and laser beam focal length were taken into account and recalculated.

Table 1 Picosecond laser beam parameters used to produce TiO_2 nanoparticles in deionised water.

Parameters	Value
Wavelength (λ)	1064 nm
Frequency (f)	200 kHz
Pulse duration (τ)	10 ps
Spot size (D)	125 μm
Scan speed (v)	250 mm/s
Laser pulse energy (E_{pulse})	45.6 μJ
Laser fluence (F_{laser})	0.37 J/cm^2

Fig. 1 Experimental set-up to produce TiO_2 nanoparticles in deionised water via a picosecond laser; λ = 1064 nm, f = 200 kHz, τ = 10 ps, and v = 250 mm/s.

2.2 Sample preparation

To characterise the nanoparticles produced using transmission electron microscopy (TEM), a copper microgrid mesh (Formvar / carbon on 200 copper mesh) was used. About three drops of the colloidal nanoparticles were deposited on the copper mesh and then allowed to dry at room temperature. During drying, the samples were covered with a transparent lid to avoid contamination by airborne dust.

2.3 Characterisation

A Transmission Electron Microscope (TEM) (JEOL 2000 FX AEM + EDX), a High-Angle Annular Dark-Field Microscope-Scanning Transmission Electron Microscope (HAADF-STEM) and Energy Dispersive X-ray Spectroscopy (EDS) (FEI Tecnai G^2 F30) were used to characterise the nanoparticles in terms of their size, size distribution and chemical compound elements. The aforementioned equipment and techniques were used to obtain images of the TiO_2 nanoparticles and their line elemental spectrum. A UV–Vis optical spectrometer (Analytic Jena, SPECORD 250, dual-beam) was used to obtain the optical absorption spectra of the nanoparticles. In addition, X-ray diffraction (XRD) (BrukerD8-Discover, step size [°2θ] = 0.0200) was used for the investigation of material crystalline structures.

3. Results and discussion

3.1 Generation of hollow TiO_2 nanoparticles

Fig. 2 (a, b) shows the TEM images of TiO_2 nanoparticles produced by picosecond laser ablation in deionised water. Some hollow nanoparticles can be observed among the solid TiO_2 nanoparticles. They were produced in the different sizes with clear boundaries. Fig. 2-c shows a histogram of the size distribution of the nanoparticles. Their sizes range from less than 10 nm to about 160 nm, with an average size of 37 nm. The ablation rate of the nanoparticles changed when the laser power was altered. In other words, the ablation rate was increased by increasing the laser beam power.
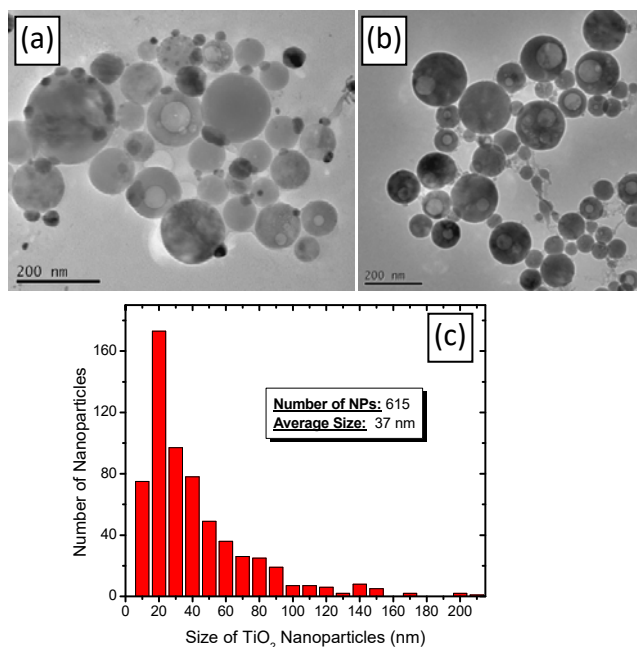
Fig. 2 (a and b) TEM images of hollow TiO_2 nanoparticles produced by picosecond laser in deionised water. (λ= 1064 nm, f= 200 kHz, v = 250 mm/s). (c) Histogram of the size distribution of the TiO_2 nanoparticles measured from 615 TEM images of nanoparticles.

As shown in Fig. 3, a range of single holes, double holes and multiple-holes were observed in the nanoparticles. In addition, some very small holes were produced in some nanoparticles, causing the nanoparticles to appear porous. It can be noted in Fig. 2 and 3 that almost all of the holes are spherical with different sizes in diameter.
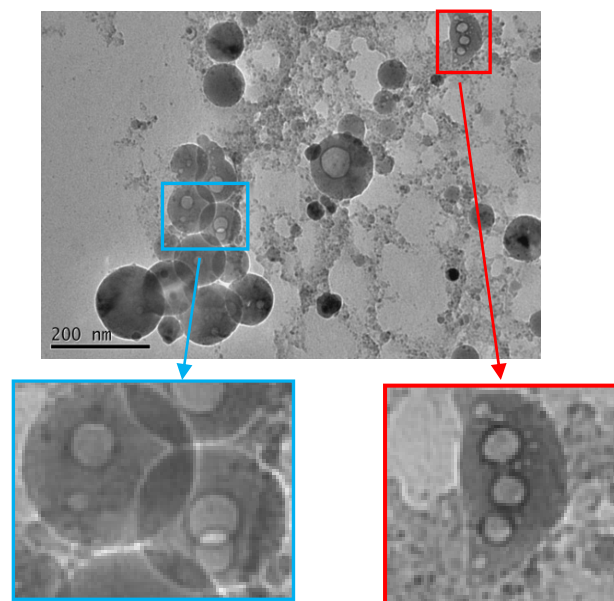
Fig. 3 TEM image of TiO_2 nanoparticles show more than one holes produced in the nanoparticles.

Picosecond laser ablation of a solid material in water is commonly accompanied by a strong plasma plume, which cools and is then condensed [17]. Condensation of the plasma plume in water leads to the generation of Ti nanoparticles. When the concentration of the nanoparticles reaches a specific value, the highly active solid Ti nanoparticles oxidise in the liquid environment, leading to the formation of TiO_2 nanoparticles in the solution. The appearance of holes in the nanoparticles may be due to the production of gas bubbles in the liquid in the vicinity of the laser focal spot on the target after laser-target interaction. This phenomenon is explained by supposing vaporised plasma plume nucleation and a preferential condensation between gas bubbles and their surroundings (water) to minimise the surface tension [18-19]. In addition to this, hollow TiO_2 nanoparticles are generated in deionised water due to the considerable increase of H_2 in TiO_2, exceeding its melting point, and the subsequent release of H_2 due to the solidification of the nanoparticles. The production of hollow nanoparticles was also observed in the generation of Ti nanoparticles in hydrogen-saturated and non-saturated ethanol due to the production of H_2 under pyrolysis of an ethanol solution [20]. The size and number of the holes in the nanoparticles depended on the amount of H in the solution, and the quantity of H depended on the permeability (P) according to Equation (1) [20]:
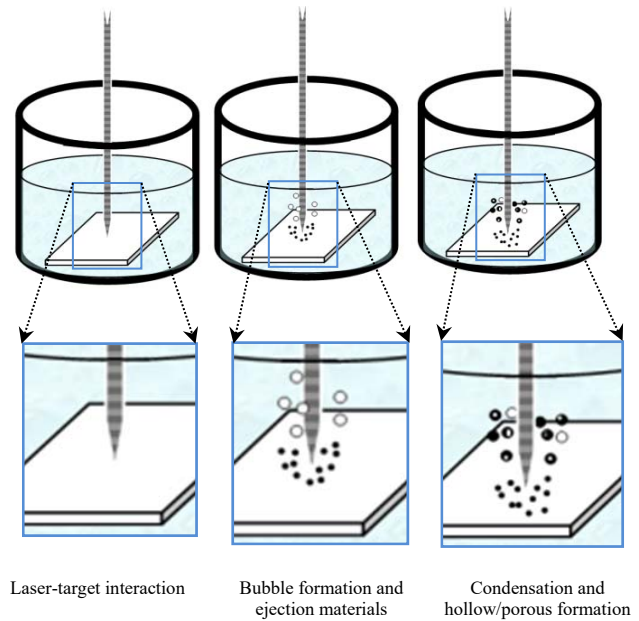
$P = DS$ _____ (1)

where D and S are the diffusion coefficient and the solubility of the hydrogen.

The mechanism of the formation of porous hollow nanoparticles is different for different methods of preparation: for example, for a hydrothermal method, the production is due to the Ostwald ripening process. This happens by changing the morphology of the material products in the solution at the reaction stages [6]. For the Kirkendall and Diffusion processes, the mechanism is based on an idealised model and a normal steady-state diffusion governed by Fick's first law of diffusion. Briefly, this entails mass diffusion and the vacancies induced by atomic concentration differences [21].

An explanation of hollow and porous nanoparticles production by laser ablation in water is due to bubble formation [22] at water-target interface during laser-target interactions. Laser ablation in a confining liquid solution can lead to a dense plasma which induces the cavitation bubbles [23]. Some of the released materials or nanoparticles from the target surface to the solution would interact with a bubble or a number of bubbles. Then as a result of condensation due to the cooling in the water environment a hole or some holes (pores) are produced in the nanoparticles. Moreover, the bubble surface pinning may occur due to ejected clusters or particles [24] (See Fig. 4), and the material detachment could be observed after collapse the cavitation bubbles in the solution [25]. In addition, holes could be produced due to the releasing of dissolved gas in molten nanoparticles while the cooling [26]. This would happen because the bubbles are produced in the water environment while the materials are ejected from the target material. In addition, during the production of nanoparticles; after shrinking of the cavitation bubbles, the material would be ejected, so the size distribution of the laser induced nanoparticles is strongly depended on the dynamics of the cavitation bubbles [25].

The porous nanoparticles might be produced due to burst of the bubbles forming high pressure jets. It is worth mentioning that hollow and porous nanoparticles are not produced in air during laser ablation [22]. During the production of nanoparticles; after shrinking of the cavitation bubbles the material would be ejected, so the size distribution of the laser induced nanoparticles is strongly depended on the dynamics of the cavitation bubbles [25].

The number of the hollow and porous structures in nanoparticles depended on the laser power because the size, lifetime and expansion speed of the cavitation bubble depended upon the laser beam parameters and nature of the liquid solution [23].

| Laser-target interaction | Bubble formation and ejection materials | Condensation and hollow/porous formation |

Fig. 4 Schematic diagram of hollow/porous TiO$_2$ nanoparticles formation.

Fig. 5 shows the HAADF-STEM and EDS images of the TiO$_2$ nanoparticles. The figures show that the amount of Ti and O material in the centre of the hole is less than those at the edges. This serves as evidence of the holes produced in the TiO$_2$ nanoparticles. The TEM images and line-scanning profile show the holes in the TiO$_2$ nanoparticles.
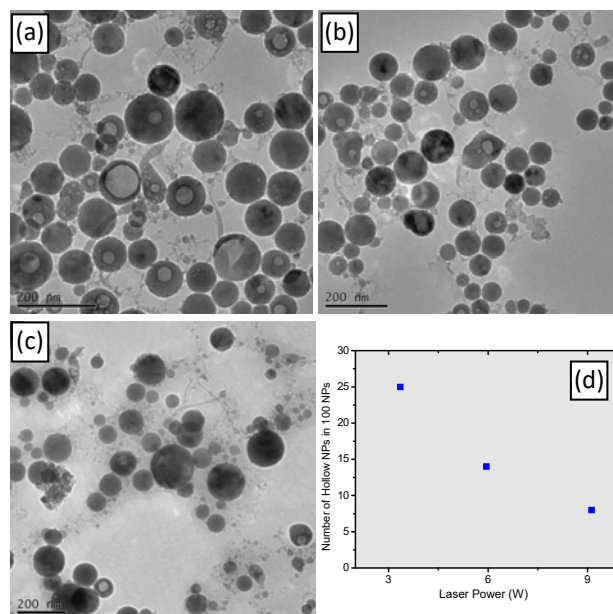
The TEM images show that the hollow or porous nanoparticles have lower material density in the middle in comparison with the edges. In addition, the holes appear lighter and the edges darker. The bright parts of the nanoparticles can be attributed to lower laser beam absorption due to a lack of the nanoparticles' composite materials. As the hollow nanoparticles are lack of materials in comparison with solid nanoparticles, they are lighter than solid nanoparticles of the same size and shape. On the basis of this fact, hollow nanoparticles are expected to have more colloidal stability than non-hollow colloidal nanoparticles due to their lower density; as a result, gravitational force has a reduced effect on the hollow nanoparticles.
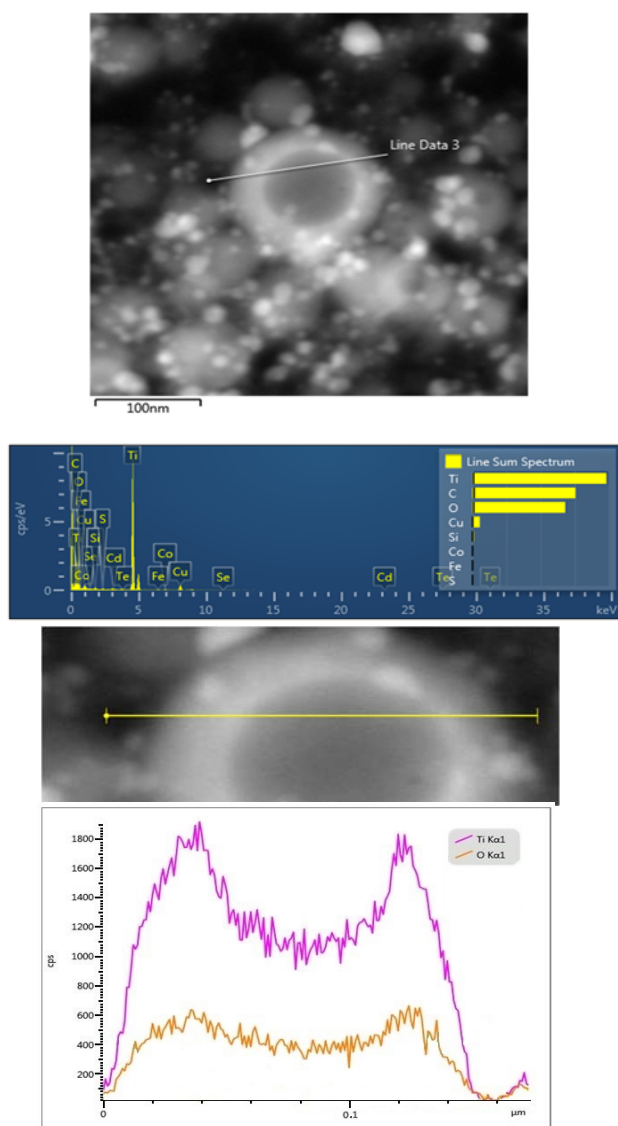
Fig. 5 HAADF-STEM and EDS images of the TiO_2 nanoparticles showing the production of hollow TiO_2 nanoparticles.

Fig. 6 TEM images of TiO_2 nanoparticles produced by picosecond laser in deionised water with different laser powers; P = 3.35 W (a), P = 5.95 W (b) and P= 9.12 W (c). Fig. (d) shows the approximate number of hollow TiO_2 nanoparticles in 100 TiO_2 nanoparticles produced at different laser powers by picosecond laser in deionised water.

3.2 Effect of laser power on the production of hollow/ porous TiO₂ nanoparticles

Fig. 6 shows TiO_2 nanoparticles produced via picosecond laser in deionised water with different laser powers: P = 3.35 W (a), P = 5.95 W (b) and P = 9.12 W (c). It can be noted that more hollow nanoparticles were generated at a low laser power (see Fig. 6–a), in comparison with the nanoparticles produced at a higher laser power (see Fig. 6 b and c). Fig. 6-d shows the number of hollow or porous nanoparticles produced per 100 nanoparticles. The number of hollow nanoparticles was roughly counted. It can be noted that lower laser powers produced more hollow nanoparticles than at higher laser powers.

Laser power has a strong effect on the production of hollow nanoparticles. A lower laser power leads to a lower temperature on the target material compares with that at a higher laser power. This leads to increased solubility of H_2 in water; in other words, more H_2-filled bubbles would be generated. It is worth mentioning that the solubility of hydrogen in liquid increases with a decrease in temperature. As a result, more hollow nanoparticles would be produced after hydrogen is released from the nanoparticles. The release rate of the hydrogen is increased (or facilitated) by increasing the temperature. This can easily occur during the production of TiO_2 hollow nanoparticles because Ti is more permeable by hydrogen [20].

3.3 Effect of laser power on the optical properties of hollow/porous TiO₂ nanoparticles

As shown in Fig. 7-a, the optical absorption spectra of hollow nanoparticles are similar at low and high laser powers. This is because the optical absorption spectrum measurement is related to the shape of the nanoparticles. Fig. 7-b shows the indirect and (c) direct energy band gaps of the TiO_2 nanoparticles produced at different laser power. In general, the energy gap was decreased with increasing laser power. At a lower laser power, the energy gap increased more rapidly than that at a higher laser power. Zhang et al. [27] found that the energy gap of the TiO_2 nanoparticles increased about 0.25 eV when their size

reduced from (5 – 50 nm) to blow 3 nm. In addition, different band gap values of the TiO_2 nano-size (Brookite) were found due to different hydrothermal times [28] or the type of nanostructure such as nano-sheets and nano-spindles [29-30].
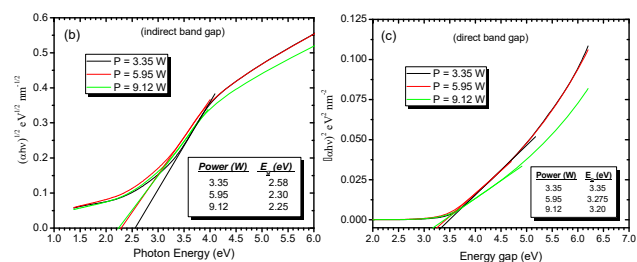
Fig. 7 Optical absorption spectra (a), indirect (b) and direct (c) band gap transition of the TiO_2 nanoparticles produced by picosecond laser in deionised water at different laser power.

The reason for the preference to hollow nanoparticles rather than solid nanoparticles in their optical properties is the thin shell of the hollow nanoparticles, which makes up inner and outer surfaces that are more effective for photocatalytic activity [9]. The photocatalytic activity depends on the thickness of the shell. So smaller nanoparticles or smaller shells would have a stronger photocatalytic activity because they have a strong absorption power [9]. In addition, the electron transfer in hollow nanoparticles to the surface area is easier than in solid nanoparticles. The electron-hole pairs face less atomic boundary (or grain boundary) while transferring the TiO_2 to its surface; as a result, they arrive faster than the solid nanoparticles.

The ability to control the proportion of hollow nanoparticles by laser power might be useful to certain applications such as energy storage devices, catalyst, optics and sensors [31]. Hollow nanoparticles produced by the laser ablation method have certain advantages over production methods because it is well known that the laser produced nanoparticles are pure and free from any chemical by-products.
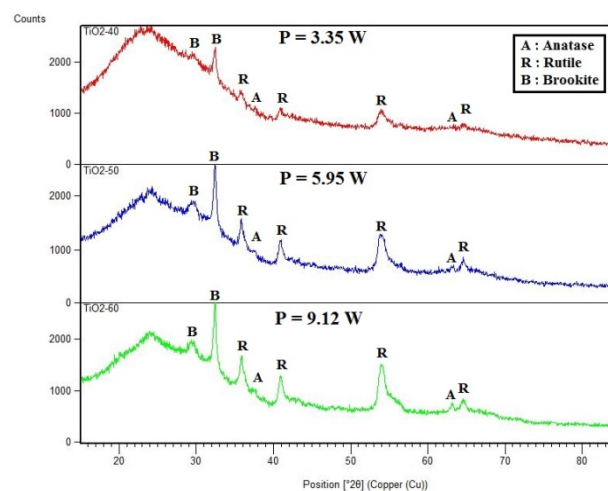
3.4 XRD of hollow/porous TiO₂ nanoparticles

Fig. 8 shows XRD of the hollow/porous TiO_2 nanoparticles produced at different laser powers. As shown in the figure, the TiO_2 nanoparticles are crystalline with mixed anatase, rutile and brookite phases. In general, the same peaks were observed in all three samples, thus the samples have the same crystalline phase, in other words, the change of laser power has no effect on the phase of the nanoparticles.

The peak positions $2\theta = 37.5$ and 63 are attributed to anatase TiO_2 phases (004) and (204) respectively [32-34].

The peak positions $2\theta = 35.8, 41, 54$ and 64.7 are attributed to rutile TiO_2 phases (101), (111), (211) and (310) respectively [34-36]. Ohshima et al. [37] observed a peak at 24 of mixed anatase and rutile TiO_2 thin film. In addition, the peak at $2\theta = 29.5$ and 32.4 are indicative of a brookite phase of TiO_2 nanoparticles [38-39].

The peaks of the sample produced at 3.35 W laser power have lower intensity in comparison with the peaks of the other samples produced at higher laser powers (5.95 W and 9.12 W) because the amount of the TiO_2 nanoparticles deposited on the 3.35 W glass slide samples was less. Less laser power produced less concentrated colloidal nanoparticles in relation to the higher laser power at the same laser irradiation.

Fig. 8 XRD images of hollow/porous TiO_2 nanoparticles produced by picosecond laser in deionised water with different laser powers; P = 3.35 W (a), P = 5.95 W (b) and P = 9.12 W (c).

4. Conclusions

Hollow and porous crystalline TiO_2 nanoparticles of 10-160 nm in size were produced by picosecond laser ablation in deionised water in a single step with a yield up to 25%. Different sizes of spherical holes in the spherical TiO_2 nanoparticles were observed. A higher ratio of hollow nanoparticles was observed among the nanoparticles that were produced with lower laser power than in those produced with higher laser power. In other words, the amount of hollow and porous nanoparticles can be controlled by manipulating the laser-induced energy. Colloidal hollow or porous nanoparticles are expected to be more stable than colloidal non-hollow-nanoparticles, due to their different quantities of material composites at the same size.

References

1. Liu, P., H. Cui, C. Wang and G. Yang: Phys. Chem. Chem. Phys., **12**, (2010) 3942.
2. Yang, G.: Prog. Mater. Sci., **52**, (2007) 648.
3. Khanal, A., Y. Inoue, M. Yada and K. Nakashima: J. Am. Chem. Soc., **129**, (2007) 1534.
4. Chaudhuri, R.G. and S. Paria: Dalton Trans., **43**, (2014) 5526.
5. Shi, S., F. Chen and W. Cai: Nanomedicine, **8**, (2013) 2027.
6. Yang, G., P. Hu, Y. Cao, F. Yuan and R. Xu: Nanoscale Res. Lett., **5**, (2010) 1437.
7. Pang, H., H. Yang, C.X. Guo, J. Lu and C.M. Li: Chem. Commun., **48**, (2012) 8832.
8. Katagiri, K., H. Inami, K. Koumoto, K. Inumaru, K. Tomita, M. Kobayashi and M. Kakihana: Eur. J. Inorg. Chem., **2012**, (2012) 3267.
9. Tsai, M.-C., J.-Y. Lee, P.-C. Chen, Y.-W. Chang, Y.-C. Chang, M.-H. Yang, H.-T. Chiu, I.-N. Lin, R.-K. Lee and C.-Y. Lee: Appl. Catal., B: Environmental, **147**, **(**2014) 499.
10. Wang, J., J. Yu, X. Zhu and X.Z. Kong: Nanoscale Res. Lett., **7**, (2012) 646.
11. Smovzh, D.V., N. A. Kalyuzhnyi, A. V. Zaikovsky, S. A. Novopashin: Advances in Nanoparticles, **2**, (2013) 5.
12. Ming, J., Y. Wu, J.-B. Park, J.K. Lee, F. Zhao and Y.-K. Sun: Nanoscale, **5**, (2013) 10390.
13. Niu, K., J. Yang, S. Kulinich, J. Sun and X. Du: Langmuir, **26**(22), (2010) p.16652.
14. Lee, S., J. Lee, S.H. Hwang, J. Yun and J. Jang: ACS nano, **9**, (2015) 4939.
15. Yang, G.-W., J.-B. Wang and Q.-X. Liu, J. Phys. Condens. Matter, **10**, (1998) 7923.
16. Yang, G. and J. Wang: Appl. Phys. A, **71**, (2000) 343.
17. Desarkar, H., P. Kumbhakar and A. Mitra: Laser Phys. Lett., **10**, (2013) 055903.
18. Semaltianos, N.G., S. Logothetidis, N. Frangis, I. Tsiaoussis, W. Perrie, G. Dearden and K.G. Watkins: Chem. Phys. Lett., **496**, (2010) 113.
19. Yan, Z., R. Bao and D.B. Chrisey: Nanotechnology, **21**, (2010) 145609.
20. Kuzmin, P.G., G.A. Shafeev, G. Viau, B. Warot-Fonrose, M. Barberoglou, E. Stratakis and C. Fotakis: Appl. Surf. Sci., **258**, (2012) 9283.
21. Fan, H.J., U. Gösele and M. Zacharias: Small, **3**, (2007) 1660.
22. Yan, Z., R. Bao, Y. Huang and D.B. Chrisey: J. Phys. Chem. C, **114**, (2010) 11370.
23. Wagener, P., A. Schwenke, B.N. Chichkov and S. Barcikowski: J. Phys. Chem. C, **114**, (2010) 7618.
24. Yan, Z., R. Bao, C.M. Busta and D.B. Chrisey: Nanotechnology, **22**, (2011) 265610.
25. De Bonis, A., M. Sansone, L. D'Alessio, A. Galasso, A. Santagata and R. Teghil: J. Phys. D: Appl. Phys., **46**, (2013) 445301.
26. Yan, Z. and D.B. Chrisey: J. Photochem. Photobiol. C: Photochem. Rev., **13**, (2012) 204.
27. Zhang, H., G. Chen and D.W. Bahnemann: J. Mater. Chem., **19**, (2009) 5089.
28. Xie, J., X. Lü, J. Liu and H. Shu: Pure Appl. Chem., **81**, (2009) 2407.
29. Lin, H., L. Li, M. Zhao, X. Huang, X. Chen, G. Li and R. Yu: J. Am. Chem. Soc., **134**, (2012) 8328.
30. Di Paola, A., M. Bellardita and L. Palmisano: Catalysts, **3**, (2013) 36.
31. El Mel, A.-A., R. Nakamura and C. Bittencourt: Beilstein J. Nanotechnol., **6**, (2015) 1348.
32. Anandgaonker, P., G. Kulkarni, S. Gaikwad and A. Rajbhoj: Chin. J. Catal., **35**, (2014) 196.
33. Almeida, L.C. and M.V. Zanoni: J. Braz. Chem. Soc., **25**, (2014) 579.
34. Ghorai, T.K: J. Mater. Res. Technol., **4**, (2015) 133.
35. Chellappa, M., U. Anjaneyulu, G. Manivasagam and U. Vijayalakshmi: Int. J. nanomedicine, **10**, (2015) 31.
36. Yan, J., G. Wu, N. Guan, L. Li, Z. Li and X. Cao: Phys. Chem. Chem. Phys., **15**, (2013) 10978.
37. Ohshima, T., S. Nakashima, T. Ueda, H. Kawasaki, Y. Suda and K. Ebihara: Thin Solid Films, **506–507**, (2006) 106.
38. Li, Y., N.-H. Lee, D.-S. Hwang, J.S. Song, E.G. Lee and S.-J. Kim: Langmuir, **20**, (2004) 10838.
39. Kandiel, T.A., L. Robben, A. Alkaim and D. Bahnemann: Photochem. Photobiol. Sci., **12**, (2013) 602.